Energy-Ball: Wireless Power Transfer for Batteryless Internet of Things through Distributed Beamforming

XIAORAN FAN, WINLAB, Rutgers University, USA
HAN DING, Xi'an Jiaotong University, China
SUGANG LI, WINLAB, Rutgers University, USA
MICHAEL SANZARI, WINLAB, Rutgers University, USA
YANYONG ZHANG, WINLAB, Rutgers University, USA
WADE TRAPPE, WINLAB, Rutgers University, USA
ZHU HAN, University of Houston, USA
RICHARD E. HOWARD, WINLAB, Rutgers University, USA

Wireless power transfer (WPT) promises to deliver energy to devices that are otherwise hard to charge or replace batteries for. This paper presents a new power transfer approach by aligning the phases of a collection of radio frequency (RF) energy chargers at the target receiver device. Our approach can ship energy over tens of meters and to mobile targets. More importantly, our approach leads to a highly asymmetric energy density distribution in the charging area: the energy density at the target receiver is much higher than the energy density at other locations. It is a departure from existing beamforming based WPT systems that have high energy along the energy beam path. Such a technology can enable a large array of batteryless Internet of Things applications and render them much more robust and long-running. Thanks to its asymmetric energy distribution, our approach potentially can be scaled up to ship higher level of energy over longer distances.

In this paper, we design, prototype, and evaluate the proposed energy transfer approach, referred to as *Energy-Ball*. We implement an *Energy-Ball* testbed that consists of 17 $N210$ and 4 $B210$ Universal Software Radio Peripheral (USRP) nodes, yielding a $20 \times 20\ m^2$ energy delivery area. We conduct carefully designed experiments on the testbed. We demo that the energy density of *Energy-Ball* at the target spot is considerably higher than the energy density elsewhere, with the peak to average power ratio of 8.72. We show that *Energy-Ball* can transfer energy to any point within the area. When the receiver moves at a speed of 0.5 m/s, *Energy-Ball* can transfer 80% of optimal power to the mobile receiver. Further, our results also show *Energy-Ball* can deliver over $0.6mw$ RF power that enables batteryless sensors at any point across the area.

CCS Concepts: • **Hardware** → **Wireless devices**; **Wireless devices**; • **Human-centered computing** → *Ubiquitous computing*;

Additional Key Words and Phrases: Wireless power transfer; Batteryless IoT; Distributed Beamforming; Mobile Receiver

Authors' addresses: Xiaoran Fan, ox5bc@winlab.rutgers.edu, WINLAB, Rutgers University, 671, U.S. 1, North Brunswick, NJ, 08902, USA; Han Ding, Xi'an Jiaotong University, Xi'an, Shaanxi, China; Sugang Li, WINLAB, Rutgers University, 671, U.S. 1, North Brunswick, NJ, 08902, USA; Michael Sanzari, WINLAB, Rutgers University, 671, U.S. 1, North Brunswick, NJ, 08902, USA; Yanyong Zhang, WINLAB, Rutgers University, 671, U.S. 1, North Brunswick, NJ, 08902, USA; Wade Trappe, WINLAB, Rutgers University, 671, U.S. 1, North Brunswick, NJ, 08902, USA; Zhu Han, University of Houston, Houston, Texas, USA; Richard E. Howard, WINLAB, Rutgers University, 671, U.S. 1, North Brunswick, NJ, 08902, USA.

2474-9567/2018/6-ART65 $15.00
https://doi.org/10.1145/3214268

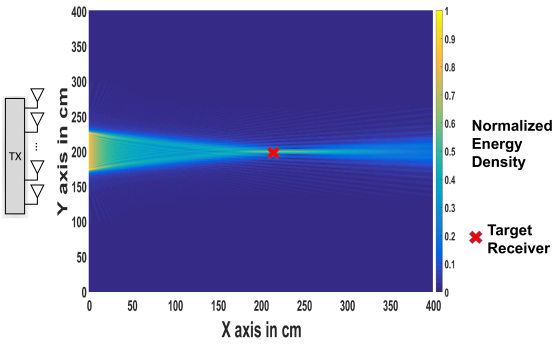

Fig. 1. Energy density distribution for beamforming.

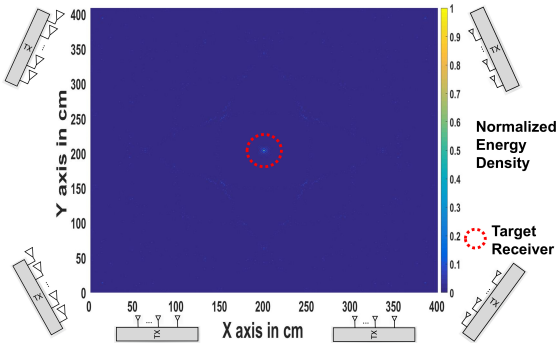

Fig. 2. Energy density distribution for *Energy-Ball*.

ACM Reference Format:
Xiaoran Fan, Han Ding, Sugang Li, Michael Sanzari, Yanyong Zhang, Wade Trappe, Zhu Han, and Richard E. Howard. 2018. *Energy-Ball*: Wireless Power Transfer for Batteryless Internet of Things through Distributed Beamforming. *Proc. ACM Interact. Mob. Wearable Ubiquitous Technol.* 2, 2, Article 65 (June 2018), 22 pages. https://doi.org/10.1145/3214268

1 INTRODUCTION

Ever since the invention of electricity, a world free of batteries and power cords has been the aspiration of many scientific investigations. Now, this vision is ever more appealing, with the proliferation of Internet of Things (IoT) systems, and at the same time ever more realistic thanks to recent advances in low-power embedded design and energy harvesting. As an example of low power IoT devices, in the year of 2016, Graule et al. [27] made a robotic drone that only needs 19mw to fly, and a couple of micro watts to remain perched on objects. Such extremely low power devices can be potentially powered through simple mechanisms such as ambient energy harvesting from lights, Wi-Fi router, TV and cellular signals [26, 39, 55]. While ambient energy harvesting has proven effective in the above examples, it becomes less effective in many other situations, especially when the required energy density exceeds what the environment offers. As such, near-field wireless charging techniques [17, 28, 34] have proven useful in delivering higher amount of energy. However near-field charging is either limited by its range or require large-scale facilities to achieve larger ranges.

As people endeavor to deliver higher amounts of energy over longer distances, they either choose to design wireless power transfer (WPT) systems using highly directional energy chargers or phased arrays that can steer the energy beam towards the target [6, 33, 34, 38]. However, such beamforming techniques have potential safety concerns as they often lead to high energy concentration along the beam, which poses risk to people or objects in those areas. Using simulations, we show the energy density distribution of an example beamforming system in Figure 1, where the energy density level along the beam is higher than that at the target receiver. As a result, a beamforming based WPT system requires extra measures to ensure (a) the energy level along the beam is low enough not to be harmful, and (b) the energy level at the target receiver is high enough to be useful.

In this paper, we set out to design a new wireless power transfer system that can focus the energy around the target and minimize energy density in other areas. Towards this goal, we arrange our transmitters in a fully distributed fashion by surrounding them around the target receiver, as shown in Figure 2. A salient property of this arrangement is that, by aligning their phases at the receiver, the energy level at the target receiver is higher than the energy level at any other spot in the charging area. In fact, a small energy ball is formed around the receiver, hence the system name of *Energy-Ball*. Figure 2 shows the energy density distribution of *Energy-Ball*

using simulation results. In designing *Energy-Ball*, we draw inspiration from the design of the surround sound system, in which multiple speakers are arranged around the audience for better audio experiences.

When devising *Energy-Ball*, we have overcome the following main challenges:

- *Realizing Energy-Ball in a Realistic Setting.* Due to its completely distributed nature, it is hard to achieve phase alignment among the transmitters, especially when the amounts of transmitters increases. In a realistic setting, these transmitters do not have phase level synchronized clocks among them , nor do they communicate with each other. Furthermore, there often exist complex multipaths where *Energy-Ball* is deployed, which makes those algorithms that rely upon channel state information (CSI) less useful.
  In this paper, we carefully address this challenge by adopting a simple yet effective phase alignment technique that is closed-loop and that does not require any CSI information. In an iterative fashion, it uses the receiver's feedback to guide the transmitter's phase adjustments towards the optimal phases, with which the maximum received power is achieved at the receiver. We achieve phase level synchronization among the transmitters through a master-slave GPS architecture.
- *Continuously Charging Mobile Target. Energy-Ball* is designed to charge devices in an IoT system, where devices may be mobile, such as low power drones/robots or sensors that are attached to a mobile platform. In order to achieve continuous charging in this scenario, we have to figure out mechanisms to continuously re-align the phases of transmitters in a timely manner.
  When the receiver moves, we need to look for a more direct way of keeping transmitter phases around their optimal values. Specifically, if the phase difference between the transmitter and the receiver was known, then the transmitter would directly adjust its phase according to the difference. Though this information is not available to the transmitter, we propose to estimate it using the phase difference between the receiver and transmitter (which can be conveniently measured by the transmitter), considering that the phase differences in these two directions are highly correlated.

In summary, our work has the following contributions:

- We have devised a new wireless power transfer system, *Energy-Ball*, that can precisely focus energy on the receiver while having low energy density at other areas. To transfer the same amount of energy to a device, such a system leads to much less RF energy in the charging area than traditional beamforming systems. We believe *Energy-Ball* provides a viable and practical charging solution to rapidly growing IoT systems. We envision that *Energy-Ball* can be deployed to surround the target IoT nodes, such as in a smart factory, warehouse, or store, delivering energy to nodes one by one before they perform the required sensing/processing/networking functions, without the need to ever replace batteries for these nodes. Moreover, *Energy-Ball* can also be used to continuously power drones or robots that are used in agriculture, rescue, industrial assembly lines [2, 4, 7].
- We have built an *Energy-Ball* testbed using USRPs and validated its charging ability and resulting energy distribution using real-world experiments. Our results show that *Energy-Ball* can deliver over 0.6 mW RF power at any point in a $20 \times 20 \times 3$ m^3 charging space, using 24 transmitters transmitting at 1.7W (which is the highest transmitting power allowed on our facility). Since *Energy-Ball* emits very low energy in the charging space, we will be able to deliver much higher energy by boosting the transmission power and/or increasing the transmitter number. Further, we show that a low-power tag [23] can be continuously powered by *Energy-Ball* at all the locations we have tried in the experiments.
- We have developed a fast phase adjustment algorithm that transmitters can adopt to continuously align their phases at a mobile receiver. For a mobile receiver whose speed is lower than 0.5 m/s, the received energy is on average around 80% of the energy received by a stationary receiver located at each point on the trajectory.

2 RELATED WORK AND MOTIVATION

2.1 Electromagnetic Radiation Based Energy Harvesting and Transferring

Many wireless charging systems transfer energy through electromagnetic radiation. We broadly group these systems into three categories: near field wireless charging, passive energy harvesting, and far field wireless energy transfer.

Near Field Wireless Charging: The near field is that part of the radiation field that is below the Fraunhofer distance $d_f = 2D^2/\lambda$ [9], where D is the source of the diffracting edge or antenna diameter, and λ is the wavelength. Transferring energy through coupling magnetic coils is a typical near-filed energy delivery system, which is also the most commercially successful wireless charging method [11, 13], ranging from charging cell phones, tooth brushes, to cars and buses. Traditionally, this method had limited charging distance and required the device be placed in a certain position [40]. Fortunately, recent development has improved their performance. Adopting the idea of closed loop beamforming, MagMIMO [34] shapes a magnet flux into a steerable beam with multiple coils to charge iPhones. Due to the nature of closed loop beamforming, MagMIMO charges the iPhone regardless of its orientation and position. Meanwhile, in 2016, Disney research has created a $54m^3$ quasistatic cavity resonance room, which can deliver up to 1900 watts of power [17] in the whole room.

In summary, near field wireless charging systems can transfer a decent amount of energy, but it either suffers from very limited charging distances or it requires special large-scale facilities to achieve larger charging ranges. Neither case is suitable for our BF-IoT scenarios.

Passive Energy Harvesting: Passively harvesting is also called ambient harvesting. It is proposed for charging sensors, medical implants and many other extremely low power sensors [36, 41, 59]. For example, Ambient Backscatter [39] is a prototype end-to-end system with the capability of harvesting energy from TV and cellular signals in the environment to activate smart cards and grocery tags. It enables ubiquitous communication between inexpensive devices that need near-zero maintenance. Talla et al. [55] harvest WiFi signal to charge low power streaming cameras and sensors. However, passive harvesting is only suitable for battery free devices that need micro watt level power, but not for IoT applications that require higher power.

Far Field Wireless Energy Transfer: Actively transferring energy to the target device has long been proposed as a promising way of transferring heftier power over longer distances. In this paper, we specifically refer to this type of wireless charging systems as WPTs. From the early Tesla's Wardenclyffe tower to the later Air Force mission of wirelessly powering an unmanned helicopter, until now people are still actively exploring new possibilities in this space. Point source far field WPT methods have lower efficiency than their near-field counterparts due to path loss, $\frac{P_r}{P_t} = G_r G_t \frac{\lambda}{4\pi d^\alpha}$, where we have α between 2 and 8 depending on the environment. For example, with an isotropic receiver and transmitter, the power transfer efficiency can be lower than 0.1% for a 10 meter charging distance. Thus, in order to deliver a certain amount of energy over 10 meters away, it is not realistic to have only one isotropic energy transmitter.

One approach to addressing this challenge is to increase the directionality of the transmission. Using directional antennas [16] or laser beams [33] can significantly increase the received energy given the same transmitting power and distance. The other approach, however, is based on beamforming, which uses a large array of transmission antennas for enhancing the signal towards certain directions. For example, Ossia [6] and Energous [10], two recent start ups, have created WPT solutions through beamforming by using a large array of WiFi band transmitters. Similarly, WPTs using distributed beamforming have also been investigated in [44, 47, 57], where closed form solutions for distributed beamforming realization and energy delivery efficiency are studied.

We take the viewpoint that far-field active transferring is the most promising approach to enabling a large array of BF-IoT systems with diversity charging energy and distance requirements. In this paper, we propose a new WPT approach that leverages a group of transmitter antennas to increase the delivered energy. Our approach,

referred to as *Energy-Ball*, is however drastically different from beamforming based WPTs in that it arranges the transmitter antennas in a completely different manner and thus yields completely different energy density distribution in the charging area. In the next subsection, we will then take a close look at the energy density distribution of these two types of WPT approaches.

2.2 WPT Energy Density Distributions and Their Implications on Safety

The risks of excessive RF energy exposure have been studied in the past, which have revealed that harmful biological effects may stem from strong RF radiation [21, 25, 32, 37, 48, 49]. High energy density across the charging space in WPT systems may cause excessive RF energy exposure, which we strive to avoid in the design of *Energy-Ball*.

Existing beamforming based WPTs have unwanted RF energy exposure along the beam. Due to path loss, the energy density on the beam path is higher than that at the target receiver. Specifically, the simulation results in Figure 1 show that on the beam path, the energy density at 1 meter away from the transmitter array is 13 times higher than the energy density at the target receiver. If the beamforming system is designed with only the received energy in mind, without realizing that the energy level on the path may become much higher, then it is hard to guarantee that the energy density on the beam is low enough to meet the FCC regulations or to be safe. FCC establishes different exposure limits for different RF ranges. These limits are codified in Title 47 of the Code of Federal Regulations (CFR). Specifically, as for conventional far field wireless charging frequency of 915MHz, maximum permissible exposure (MPE) for uncontrolled environment is $0.6mw/cm^2$ [12]. In addition, due to skin depth effect [43], WPT systems operating at higher frequencies naturally interact more strongly with the human body than lower frequency WPTs [1].

Clearly, guaranteeing safety is one of the key objectives when designing a wireless charging system, especially those that can work over several meters or longer [44]. A safe WPT approach has been investigated in [19]. In this work, under the MPE constraint, the proposed approach selects specific energy chargers for a given set of available energy chargers. On the other hand, a laser based wireless power transfer approach is proposed in [33], where it automatically detects people in its laser beam path and turns the laser beam off. In *Energy-Ball*, as shown in Figure 2, the peak energy exists precisely at the target receiver, an it is much higher than the received energy at other locations. Thus, by controlling peak energy level at the receiver at a proper level, the entire charging area should also be safe.

3 *ENERGY-BALL* DESIGN DETAILS

3.1 Overview

We have two main objectives when designing *Energy-Ball*:

(1) **Precise Wireless Energy Transfer:** Taking a significant departure from beamforming based WPT systems, *Energy-Ball* arranges transmitters around the target devices, like speakers in a surround sound system. When these transmitters align their phases at the target, an energy ball is precisely formed around the target. The received energy density at the target is maximized while the energy density elsewhere is kept low.
(2) **Charging Mobile Receiver:** We design an adaptive Kalman filter based framework to quickly re-align phases for mobile receivers. Based on the fact that phase differences between transmitters to the receiver and the receiver to transmitters are correlated, transmitters can estimate the needed phase differences for phase alignment by using their measured phases. Transmitters then adapt their phases locally.

3.2 Energy Transfer through Phase Alignment

Energy-Ball has two main components. Firstly, we arrange the transmitters around the target receiver (we will discuss the spatial relationship between transmitters and receiver later in this subsection), and secondly we align their phases at the receiver.

There are various approaches to aligning the transmitter phases. In our implementation, we extend the algorithm presented in [46]. We partition time into rounds of equal duration, and within each round, every transmitter transmits energy to the receiver at several randomly chosen phases, and expects a feedback beacon from the receiver at the end of the round indicating whether any of the phase combinations gives higher energy than in the previous round. After receiving the feedback, the transmitters choose a phase combination that has given the highest energy level at the receiver, and then performs next round of random phase adjustments around this combination. Repeating this process round by round, the receiver can guide transmitters to adjust their phases towards the optimal phase combination which gives the optimal energy at the receiver. This algorithm does not need complex channel state estimation, and it naturally takes into consideration the multipaths in the environment. Though a heuristic based approach, it always led to fast convergence in many experiments we have conducted on our testbed, mostly because our transmitters emit sine waves which have rather smooth slopes around the peak region. More details on the implementation of our phase alignment algorithm will be further presented in Section 4.2.

Can We Form an Energy Ball? Our simulation results show that when all transmitters align their phases at the receiver, we can indeed form an energy ball at the receiver. That is, the energy density at the target is higher than the energy density at any other location within the charging area. For example, in the results presented in Figures 3 (a) and (b), we place 100 transmitters equally spaced on the edge of a circle with a radius of 10m, and place the receiver at the center of the circle. Transmitters are isotropic, emitting narrow band RF signal at 1GHz. Signals are coherently added up at the target receiver. Figures 3(a) and (b) pictorially show the energy density distribution in a 10×10 meter area around the target receiver in free space and multipath environment (with GWSSUS multipath channel [42]), respectively. In both settings, we witness a sharp energy peak around the target receiver (circled using dotted red circle, the same for other energy distribution simulations). Specifically, the peak to average energy ratio in the free space case is 90.9, while the peak to average energy ratio in the multipath scenario is 81.1. Further, Figure 3(c) shows a 3D view of the resulting energy ball and the corresponding transmitter deployment.

Besides having simulation results and actual experimental measurements that show the energy ball, we have also mathematically proved that the energy at the target receiver is indeed the maximum energy across the entire charging area. Interested readers are referred to [22] for detailed proof. Note that in practice, if the number of transmitters is too small (say, 4 transmitters) or the receiver is placed far outside of the transmitter area, the received power at the target location might not be the maximum received power across the entire space. However, this observation still holds in most of the practical settings, as we will later show in Section 5.1.

How Small is the Energy Ball? Considering an asymptotically large number of transmitters, we have verified in [22] that the distance between the point that receives the maximum energy level and the first point that receives half of the maximum energy, which is usually called 3dB-down distance (d_{3dB}) in communication, is:

$$d_{3dB} \approx 0.22\lambda. \tag{1}$$

We can use d_{3dB} to represent the size of the energy ball, which is proportional to the RF wavelength we use for charging. For an operating frequency of 1GHz, d_{3dB} is around 13cm, which is quite focused. Further, through simulation studies, we find that even for a smaller number of transmitters or asymmetric transmitter placement, d_{3dB} would still be a fraction of λ as long as transmitters are placed around the target receiver.

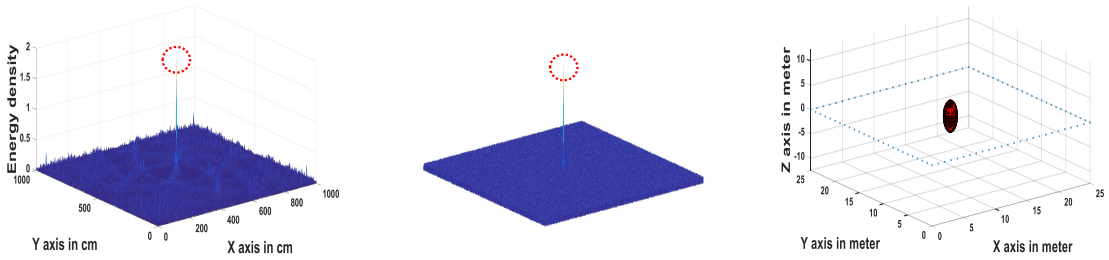

Fig. 3. When we place the receiver in the center of the transmitter square, (a) shows the energy distribution around the receiver in a 2D plane and (b) energy distribution under a GWSSUS channel, (c) pictorially shows the 'energy ball' relative to transmitters in a 3D space, where blue dots mark the transmitters.

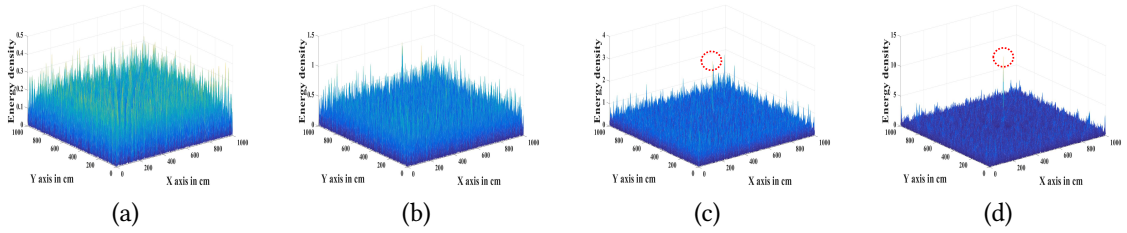

Fig. 4. Simulated energy distribution around the the target receiver (target receiver is placed at the center) with (a) 8 transmitters (b) 16 transmitters (c) 25 transmitters (d) 50 transmitters.

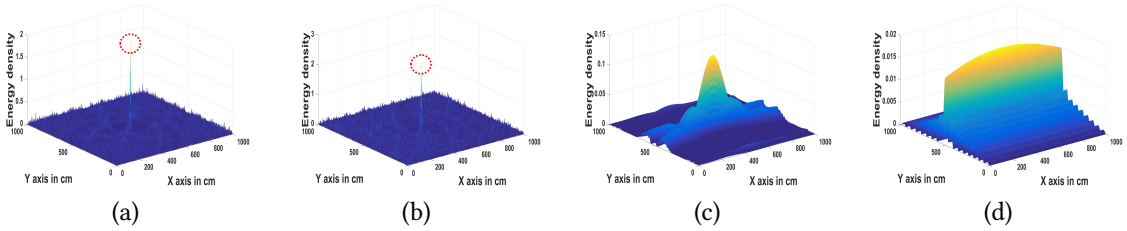

Fig. 5. Energy level distribution in different transmitter-receiver placement settings: (a) receiver placed at the center of transmitter square; (b) receiver placed in the transmitter square, but not the center; (c) receiver placed outside of transmitter square, but close; (d) receiver placed further away to the transmitter square. Among these four cases, the energy ball is formed in the first three case.

How Many Transmitters We Need to Form the Energy Ball? In the above simulation studies, we have 100 transmitters. In reality, deploying such a large number of transmitters is not only prohibitively expensive, but will also be hard to achieve synchronization/phase alignment among them.

Figures 4(a)-(d) show simulation results of the energy density distribution around the target receiver with different transmitter numbers. In these simulations, transmitters are still placed on a circle centered around the receiver. The results show that no matter how many transmitters we have, the energy level at the receiver is the

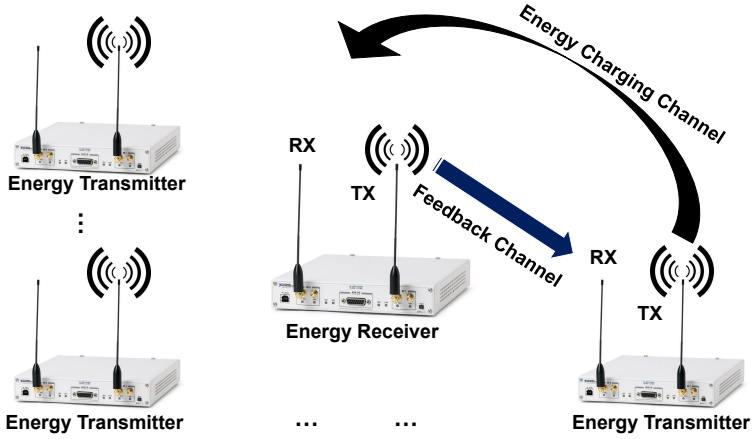

Fig. 6. Each radio device has separate ports for transmitting and receiving. We define the channel from the transmitter to receiver as 'energy charging' channel, and the channel from the receiver to transmitter as 'feedback' channel. These two channels work at different frequencies but are correlated.

highest. Further, when we have 25 transmitters, the peak to average energy ratio is already 13.4. In practice, we built an actual testbed consisting of 24 transmitters, and we will show later in section 5 that the energy at the receiver is indeed considerably higher than any other spot.

Does the Receiver Need to be Placed at the Center? We have shown one can form a tight energy ball around the target receiver when placing the target receiver at the geometric center of the transmitters. We next investigate the impact of receiver placement using simulations, in which we consider 100 transmitters that are equally spaced along a 25×25 meter square. We vary the location of the receiver, and look at the energy distribution within a 10×10 meter area around the receiver, which are shown in Figures 5(a)-(d).

In Figure 5(a), the receiver is placed at the center of the square. In Figure 5(b), the receiver is placed within the square, but not at the center. In Figure 5(c), the receiver is placed outside of the square, but its distance to the square is comparable to the length of the side (its distance to the center of square is 85 meters). In Figure 5(d), the receiver is placed far away from the square (its distance to the square is 200 meters). We observe that, as long as the receiver is within the square, the energy concentration around the receiver is quite narrow, hence precise energy delivery. Once the receiver is outside of the square, the width increases. However, we consider the energy distribution in Figure 5(c) still precise, but not in Figure 5(d). Through extensive simulations, we observe that, not only do we not need to place the receiver exactly at the center, but the key to precise energy delivery is that *the distance between transmitters and receiver is comparable to the distance between transmitters.* The reason is, when the distance between the transmitters and receiver is much larger than the distance between the transmitters themselves, the setup approaches traditional beamforming and loses the advantage of *Energy-Ball*.

3.3 Charging Mobile Receiver

The second salient feature of our system is the ability to focus energy to devices while they are moving. Below we discuss how we manage to charge mobile receivers.

3.3.1 Channel Reciprocity and Channel Correlations. The key to charging a mobile receiver is the ability to quickly focus the transmitters' phases at the new location of the mobile receiver as it moves. In order to ensure smooth re-alignment, it is important to align each transmitter's phase in a timely manner. Indirect methods such

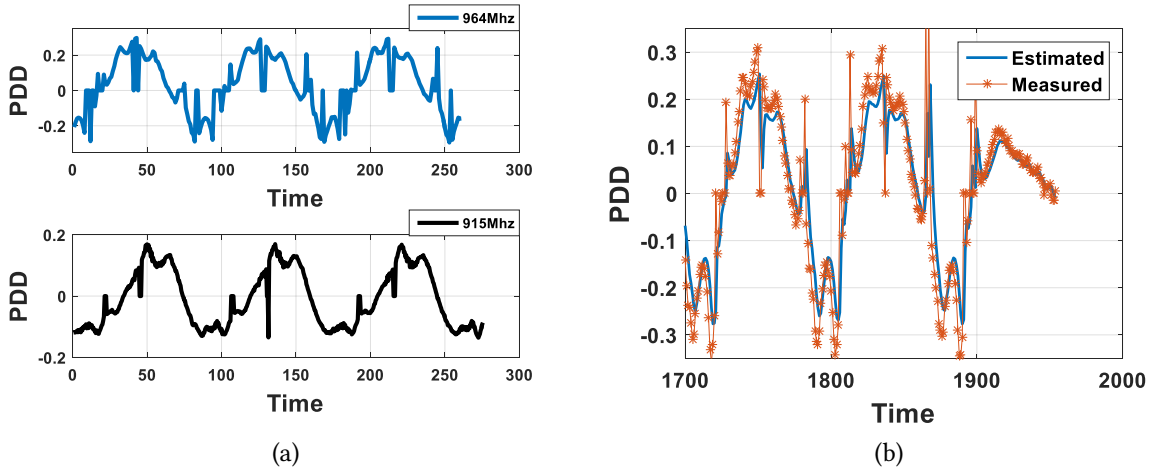

Fig. 7. (a) PDD at 915MHz and 964MHz channel. Measurement results indicate the PDDs are correlated for these two different channels. (b) Estimated energy charging channel PDD from the adaptive Kalman filter. We also show the measured energy charging channel PDD as the ground-truth. This result suggests our phase estimation algorithm for mobile receiver is indeed accurate.

as inferring phase differences by observing the Received Signal Strength (RSS) value at the receiver [46], are not sufficient because the convergence process may take tens of seconds. Meanwhile, sequential methods in which each 's phase is adjusted one by one [50, 54] are also not fast enough.

In this study, we deal with this problem as follows. If we assume all the nodes are synchronized, and the channel is time invariant, then the link from the energy transmitter to receiver (referred to as the energy charging channel) and the link from the receiver to transmitter (referred to as the feedback channel) are **reciprocal** – the absolute values of phase differences on these two channels should be the same [29, 30, 35, 58]. Hence phase alignment can be quickly realized by taking advantage of channel reciprocity. Specifically, we can have the receiver broadcast pilot beacons to all transmitters, such that each transmitter can measure the phase difference and then adjust its phase locally according to the measured phase difference.

Unfortunately, the above method requires the two channels to be strictly reciprocal, which in turn requires all the nodes to work in a dedicate Time Division Duplex (TDD) fashion[1]. That is, both the transmitter and receiver should have an antenna that can switch between receiving and transmitting without re-locking its phase. The TDD mode requires a specifically designed hardware that is not readily available on most low-cost IoT nodes. Instead, it is more often that nodes work in the Frequency Division Duplex (FDD) mode. As shown in Figure 6, in this setting, each node will use two RF ports, one for transmitting and the other for receiving, both working simultaneously but at different frequencies. These two ports are spatially separated but close to each other.

Perfect channel reciprocity does not hold in our case since the energy charging channel and the feedback channel work in different frequency bands that have different multipaths [18, 31]. However, considering the fact that the two ports on a node are very close, and the receiving antenna and transmitting antenna on the energy receiver move in a correlated trajectory, we have the hypothesis that the phase difference values for these two channels are highly correlated.

[1]The full duplex radio is the best candidate to align phases using the channel reciprocity, however it involves even more complex hardware and software design.

We have conducted experimental investigations to confirm this hypothesis. Specifically, we use two USRP N210s and configured each USRP to transmit and receive using two different antennas. The two USRPs are synchronized by GPS where one is transmitting at 915MHz and receiving at 964MHz while the other is transmitting at 964MHz and receiving at 915MHz. Then we attach the two antennas of the receiver USRP to a rotor, which spins at a constant speed of 0.4m/s. Figure 7(a) shows the measured phase difference derivatives (PDD) –the differences between adjacent phase difference values for a feedback rate of 20Hz – at different frequencies. We observe that the two channels' PDD values exhibit strong correlation and have similar trends. Hence, we believe our hypothesis is true and can estimate the phase differences at the energy charging channel using the phase differences from the feedback channel. As such, transmitters can measure the phase difference on the feedback channel, estimate the phase difference on the energy charging channel, and then adjust their phases locally to achieve rapid phase alignment.

3.3.2 Phase Estimation Using Adaptive Kalman Filter. We adopt an adaptive Kalman filter based estimation method. On a transmitter node, we can model the received beacons as a state space model, in which y_n denotes the n-th feedback channel PDD, and x_n denotes the n-th energy charging channel PDD. We have the following:

$$x_{n+1} = Ax_n + w_n, \quad y_n = Cx_n + v_n. \tag{2}$$

The signals w_n,v_n are mutually-independent, zero-mean, white-noise signals with covariance matrices Q_n and R_n: $E[w_n w_i^T] = Q_n\delta_{ni}$, $E[v_n v_i^T] = R_n\delta_{ni}$, and $E[w_n v_i^T] = 0$.

We first use our observed x_n and y_n data for pre-processing. Specifically, the initialization Kalman filter parameters $\theta = [A, C, Q, R]$ are calculated by Expectation Maximization (EM) [20] algorithm from the pre-processing data. Next, in order to timely estimate x_n, we pass y_n through the initialized Kalman filter and adopt EM algorithm to adaptively update the Kalman filter parameters $\theta = [A, C, Q, R]$ periodically. Specifically, each transmitter estimates and adjusts its new energy charging channel PDD x_n upon receiving a feedback beacon, and each transmitter updates its Kalman filter parameters using EM algorithm upon receiving every M beacons. In this way, each transmitter can locally adjust its phase to achieve rapid phase alignment. Figure 7(b) shows an example PDD estimation sequence. The estimated energy charging channel PDD values (blue curve in Figure 7(b)) are in close agreement with the measured PDD values (orange dots in Figure 7(b)). In this experiment, the average PDD estimating error is 2.4 degree, which is more than enough for achieving distributed phase alignment for our purpose[2].

4 BUILDING *ENERGY-BALL* TESTBED USING USRPS

In order to implement and evaluate the *Energy-Ball* design presented in Section 3, we develop an actual testbeb consisting of 17 N210 and 4 B210 USRP nodes.

4.1 Testbed Setup

USRP Deployment and Configuration: We deploy 16 USRP N210 and 4 B210 as transmitters, which are mounted on the 3-meter high ceiling of our laboratory, forming a $20 \times 20\ m^2$ area. Another N210 acts as the receiver in our testbed. It keeps broadcasting feedback beacons to all transmitters to guide their phase adjustments towards the optimum. Our working frequencies are 915 and 964 MHz in this study. The maximum output power for each transmitter in our testbed is around $71mw$ ($18.5dbm$). We use a WBX RF daughterboard on the USRPs. There are two RF ports on each N210 and four RF ports on each B210, in total we have 24 transmitters. Transmitters and the target receiver work in FDD (with different antennas for transmitting and receiving) full duplex mode. The energy charging channel is set as 915MHz narrow band, and the feedback channel is set as 964MHz.

[2]Through simulations, we find that as long as the transmitter's phase is within 45 degrees of the optimal phase, *Energy-Ball* can still reach at least 90% of the optimal energy at the receiver. Hence, we do not require the transmitter phases to be exactly the optimal value.

Fig. 8. Real world *Energy-Ball* testbed.

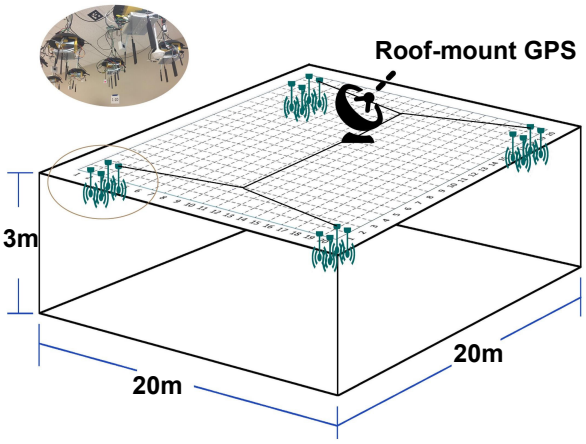

Fig. 9. The illustration of *Energy-Ball* setup.

The receiver is set up on the floor, and the receiving antenna is attached to our specifically designed robot, making it easier to change the receiver location. Transmitters' antennas are fixed, TG.35.8113 in our testbed, with quasi-isotropic radiation patterns and low return loss in 915 and 964 MHz. The testbed itself is shielded from outside, but the indoor RF multipath situation is quite complex. Our testbed is housed in a cluttered laboratory, with floor, walls, and ceiling made of high reflection materials.

Figure 9 shows a typical testbed deployment, 4 *N*210s and 1 *B*210 at each of the four corners of the ceiling, with 1 meter between them. There is no communication channel between the transmitters. We could place the receiver anywhere in the deployment area.

GPS Synchronization: We synchronize the transmitters through a master-slave GPS system. Specifically, we use a rooftop-mounted GPS antenna that provides reference signals (as the master clock) to the indoor GPS splitter. An Octoclock-G unit containing a GPS disciplined oscillator (GPSDO) generates the PPS and 10MHz reference signals which are distributed via equal length cables (75ft + 7.5ft) to 8 other Octoclock units which do not have GPSDOs. Four of these Octoclock units are installed in the corners of the testbed to split the reference signals using equal length cables (10ft). The use of equal length cables and a symmetric topology ensures that all connected devices will see the same reference signals with little deviation in phase and time.

Distributed Phase Alignment: How to achieve phase alignment is orthogonal to the design of *Energy-Ball*, and we can potentially pick any practical phase alignment algorithm. In this study, we build our phase alignment algorithm on the 1-bit phase alignment algorithm that is proposed in [45, 46]. That is, upon receiving a 1-bit feedback from the receiver, transmitters will randomly adjust their phases. The energy receiver will measure the resultant energy level, and send a feedback to indicate if this phase adjustment has led to a better received energy. If yes, the transmitters adopt this new phase combination; otherwise, they continue to use their old phase combination. In either way, at the end of each round, the transmitters keep the best phase combinations they have attempted thus far. Repeating this process, the transmitter phase combinations will approach optimal values that result in the optimal energy level at the receiver. In this study, we extend the 1-bit phase alignment algorithm. In each round, instead of trying one phase adjustment, the transmitters try N different phase adjustments. The receiver will then notify the transmitters whether any of the N new phase combinations gives higher energy then the old phase combination; if yes, which new phase combination is the best.

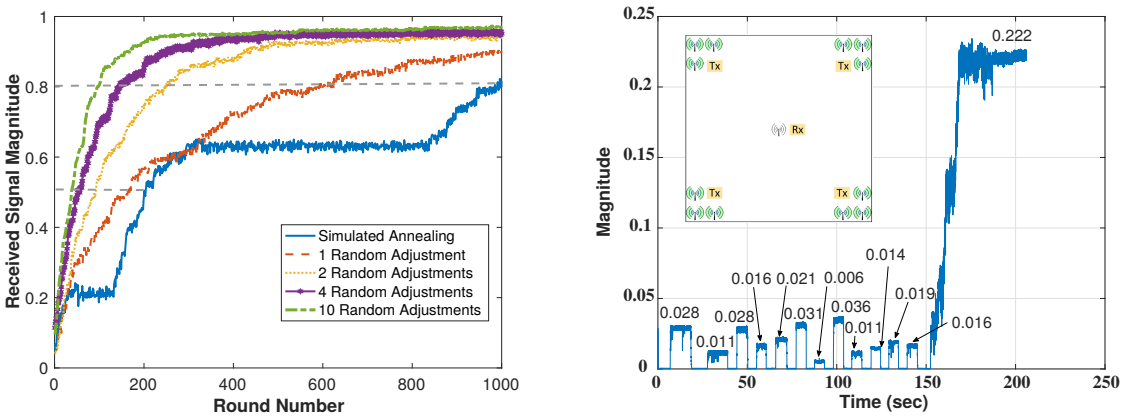

Fig. 10. (a) Convergence speed comparison for algorithms in different random adjustments N and simulated annealing. Phase alignment with larger N converges faster. (b) In the first 150 seconds, we turned on/off and measured 12 transmitters one by one. After time 150, we turn on all transmitters and started phase alignment. RSS quickly converges after that.

Our extension converges much faster compared to the 1-bit algorithm. Figure 10(a) shows simulation results (with 100 transmitters) of convergences for several different N values, with the simulated annealing algorithm [56] and 1-bit algorithm ($N = 1$) as baseline results. The results show that the convergence is significantly faster than base line algorithms with larger N.

Figure 10(b) shows an example experiment of real world distributed phase alignment. There are 12 transmitters in this experiment, the feedback rate is 20Hz and $N = 2$. In this experiment, we turn on and off 12 transmitters one by one to record the RSS contribution from each transmitter in the first 150 seconds. After 150 second, we turn on all transmitters and run the phase alignment algorithm. The RSS converges to near optimal after 9 seconds. Specifically, the optimal RSS is 0.222, and *Energy-Ball* reaches of the optimal RSS in this experiment.

4.2 GNU Radio Implementation

Signal processing tasks are performed by the GNU radio version 3.7.6.1. An overview of implementation flow for transmitters and the receiver is illustrated in Figure 11. We write multiple out-of-tree GNU radio modules to implement our functions. We next describe the GNU radio signal processing flow in detail.

4.2.1 Transmitter Side: The transmitters first receives feedback beacons in a narrow band 964 MHz channel by a USRP Hardware Driver (UHD) source block. Then after low pass filtering, the transmitter demodulates the incoming signal using the preset width-value mapping and guard band design in the demodulation block. By changing the threshold parameter on this block, we can calibrate the threshold that differentiates noise and beacons at the beginning of each experiment. This is important since the experimental environment is changing with time. The transmitter will do different tasks according to the demodulated beacons.

Stationary Scenario: The transmitter applies N phase adjustments after demodulating the beacon in the next block. Note that the transmitter holds its phase for the period of a slot τ, $\tau = t/N$, where t is the duration for a round, we set $t = 50ms$ in our testbed. Due to the complexity involved in having large N values, we implement $N = 2$ in our testbed. At last, after an output control block, the transmitter sends out the narrow band 915 MHz phase adjusted signal by a UHD sink block.

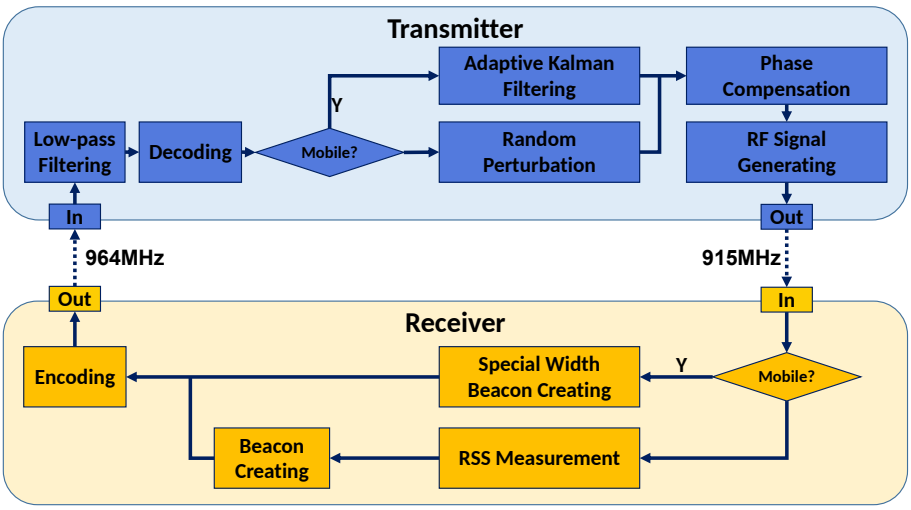

Fig. 11. *Energy-Ball* TX and RX signal processing flow.

Mobile Scenario: The transmitter measures the phase difference of each incoming beacon and calculates the PDD accordingly. Within each incoming beacon, every two adjacent samples will yield out a phase difference, and the phase difference of this beacon is calculated by averaging the phase difference of all adjacent samples. Since USRP could only calculate wrapped phases, we apply Fast Fourier Transform (FFT) for each beacon to do phase unwrapping before calculating the phase difference.

Then the calculated PDD is sent to the Kalman filter to estimate the PDD of 915MHz channel. Lastly the transmitter adjusts its current phase using this estimated new phase. The Kalman filter parameters are updated by the EM algorithm once for every 60 beacons.

4.2.2 Receiver Side: The receiver acts as a coordinator for transmitters, sending out instructions to guide the transmitters' phase adjustment towards constructive interference among them. By broadcasting different beacon width, the receiver sends different beacons to indicate if its stationary or mobile.

Stationary Scenario: The receiver first receives all incoming signals in a narrow band 915 Mhz channel. In the following block, after low pass filtering, the receiver measures the received energy by averaging the RSS of all incoming signals for each of the N phase adjustments. It sends out an instruction to the next block at the end of each round after comparing the average RSS values for each phase combination, telling the next block which phase adjustment in this round has the highest energy. Then, the next block modulates a width-based beacon following the preset width-value mapping. Finally, this beacon is sent out by the last UHD sink block in a narrow band 964 MHz channel. In our system, the receiver broadcasts 20 beacons every second. Hence it has to process receiving signal every 50 milliseconds.

Mobile Scenario: In this case the receiver keeps broadcasting 20 special width beacons every second. Transmitters measure the phase difference of 964MHz channel according to this beacon.

4.2.3 Robust Pulse-width Modulation Feedbacks. Next, we take a closer look at the feedback mechanism for the receiver. In the feedback control phase alignment method, the receiver sends feedbacks to transmitters to

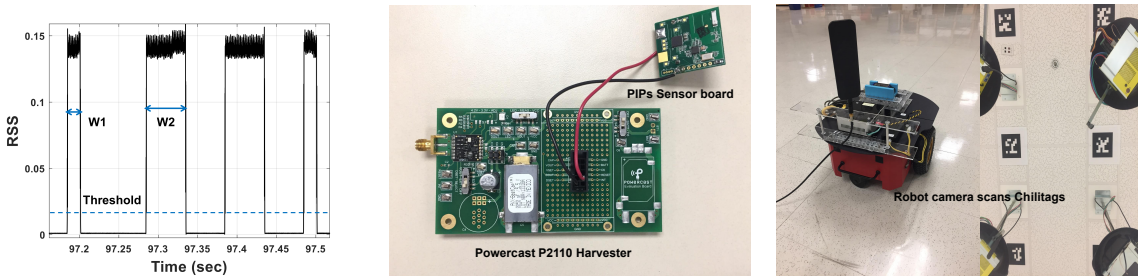

(a) (b) (c)

Fig. 12. (a) We use different beacon width to indicate feedback information. Only one threshold is used to differentiate environmental noise and beacons. (b) Powercast P2110-EVB board and our PIPs sensor board. (c) Energy measurement robot scans Chilitags (on the ceiling) for navigation.

signify which phase combination out of the $N + 1$ options gives the strongest signal to the receiver. Below, we use $N = 1$ to simplify the discussion. In this case, the feedback has two values, 0, meaning the transmitter should use its old phase value, and 1, meaning the transmitter should adopt the randomly picked phase value. In [52], the receiver feedback uses signal amplitude to modulate: low amplitude denoted as 0 and high amplitude denoted as 1. Such a scheme requires two preset amplitude thresholds, one threshold for differentiating noises and valid feedback beacons, while the other for differentiating lower amplitude from higher amplitude. Choosing suitable amplitude threshold values, however, is quite challenging as different settings have significantly different radio environments; even the same setting may experience considerable fluctuation with time. Also, N feedback control phase alignment method needs $N + 1$ vulnerable thresholds, which is extremely difficult to realize while the receiver is moving. In [53], a GMSK-based feedback scheme is used, which only requires one threshold to differentiate noise from feedback beacons. On the downside, it requires phase-level synchronization among the transmitters and receiver, which is not always available in such a distributed system.

In order to address this issue, we choose to adopt a width-based modulation method and show that it is simple but robust. In each round, the receiver broadcasts a feedback beacon that has $N + 2$ possible widths, in which $N + 1$ different widths are for feedback control phase alignment method while the receiver is stationary and another special width is used for adaptive Kalman filter while the receiver is mobile. The mapping between beacon width and specific values is pre-determined and known to each transmitter and receiver. After receiving a feedback beacon, transmitters infer its value based upon the beacon width and the pre-determined mapping. It is very likely that the received beacon width does not exactly match any of the preset values, and so we set a small tolerance space $\delta = \pm\frac{d}{5}$, where d is the expected beacon width, as a guard band (in time domain) to address this problem.

Compared to amplitude-based feedback beacons, width-based beacons are more robust since they only needs one threshold to decode the feedback (the threshold differentiating environmental noise and receive beacons, shown in Fig 12(a)). We note that the downside of the width-based beacon scheme is the relatively limited beacon values it can support, which is not a concern in our system because large N values are not realistic anyway.

4.3 Experimentation and Measurement Tools

4.3.1 Energy Harvester and Low-Power IoT Sensors: In the testbed, we utilize the delivered energy to power an in-house low-power IoT sensor, PIPs [23, 24, 60], which has been designed for smart building applications.

Figure 12(b) shows the PIPs board and the energy harvester board. A Powercast P2110-EVB [8] serves as the energy harvester in our system. It converts input RF energy into DC energy, charging a 500uF capacitor on the

P2110-EVB board. The output voltage of P2110-EVB is then set as 3.3v by a regulator and the regulator will only be turned on when the voltage across the capacitor exceeds 1.2v. The regulator consumes the stored energy in the capacitor. Note at 915Mhz, the P2110-EVB energy harvester has around 50% RF-DC efficiency. Hence the actual rectified DC power received at the end device is less than the absolute delivered RF power.

We charge PIPs by using the 3.3v output voltage. An Agilent E4405B [5] is used to measure the absolute incoming RF signal strength. Though the harvester could be turned on as long as its input RF signal strength is over -12 dbm, around -7 dbm signal strength is needed to make the regulator work continuously. Otherwise, voltage between the capacitor pins would drop while powering the regulator, hence failure to provide a stable 3.3v output voltage.

PIPs is an ultra low-power sensor board, consisting of a moisture, temperature, and magnet open/close sensor. Normally, PIPs is powered by a coin cell. Here we configure PIPs such that it collects and reports data every 10 seconds. It takes 45.7 μJ to collect and transmit data, and consuming 3 μW to stay idle.

In order to charge PIPs, we first attach the receiver N210's antenna onto a tripod with a coax cable and run feedback control phase alignment method to achieve the optimal energy at the receiver. Next, keeping the receiving antenna in the same location, we connect it to the P2110-EVB harvester board that converts the received RF energy to DC energy. As soon as sufficient energy is generated, PIPs would start transmitting sensed data to its receiver.

4.3.2 Energy Measurement Robot: Figure 12(c) shows a picture of our energy measurement robot and Chilitags on the ceiling. The robot is controlled via ROS (Robot Operating System) [51] and it's a Pioneer-p3dx robot [14]. The robot is differentially driven, and uses a Logitech c920 webcam for localization via the Chilitags library [15]. There are approximately 460 11" by 11" fiducial markers placed in a grid on the ceiling with a one meter spacing. For the purposes of this experiment, the robot was controlled via teleoperation, though it is designed to be operated autonomously. The Rosaria package provides a ROS compatible interface to the robots on-board controller, allowing any other program in the ROS ecosystem to communicate with it. A simple logger was created in python to record the robots position, and plot the path that the robot followed during the experiment.

4.3.3 Spectrum Analyzer and USRP Calibration: We use a spectrum analyzer Agilent E4405B to measure the absolute RF channel power. The spectrum analyzer can be used for acquiring absolute channel power on USRPs. USRPs can only measure RSS without units. But since the RSS measured on USRPs and their daughterboards is linear to the absolute RSS [3], we can figure out the absolute measured power on a USRP by calibration. Specifically, we set a USRP N210 broadcasting RF energy constantly, and we connect the receiving antenna to a calibrated spectrum analyzer through a coax cable to measure the narrow band 915 MHz channel power. While keeping the receiving antenna at the same location and RF source USRP broadcasting the same signal, we then disconnect the coax cable from the spectrum analyzer and connect this cable to the receiving RF port of another USRP. By this calibration process, we can map the unitless USRP measured RSS to the absolute power (in Watt).

However, we note that our calibration process does have limitations. For instance, the receiving RF port on USRP N210s most likely saturates if the received RF power exceeds 9dBm (around 7.9 miliwatt), in which case the USRP likely loses its linearity between the recorded RSS and the absolute received RF power. As a result, we limit the received power accordingly in our experiments.

5 EVALUATION

Using the USRP-based testbed, we have conducted thorough and carefully designed experiments to evaluate the proposed merits of *Energy-Ball*. We also demonstrate *Energy-Ball* can charge PIPs sensors across the room, enabling battery free IoT communication.

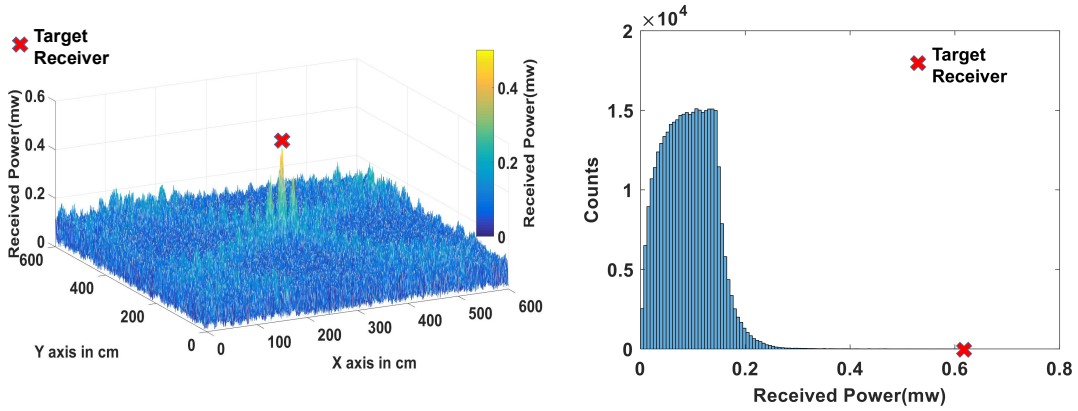

(a) (b)

Fig. 13. Using the topology shown in Figure 9, we measure the power level distribution of *Energy-Ball* in a 6×6 meter area centered at the receiver. (a) presents the 3D view of distribution, while (b) presents the histogram of the power level measurements. The distribution clearly shows that the energy density level at the receiver (marked by the red X) is much higher than that at other spots within the measurement area.

5.1 Energy Density Distribution of *Energy-Ball*

First, we measure the energy density distribution in the charging area. We show that with *Energy-Ball*, the energy level at the target receiver is the maximum across the entire area. We have also implemented a traditional beamforming based WPT system and compare its energy distribution pattern with *Energy-Ball*.

Experimental Setup: We use the topology shown in Figure 9 for *Energy-Ball* implementation in this experiment. On the other hand, for comparison, as shown in Figure 14(a), we custom build a beamforming rack which has 16 transmitting antennas and 16 receiving antennas to perform MRC [38] beamforming based WPT.

The main challenge in conducting this experiment is measuring the energy distribution in the area. Manually sampling the area would take a significant amount of time (e.g., tens of hours), and it is very hard to keep the

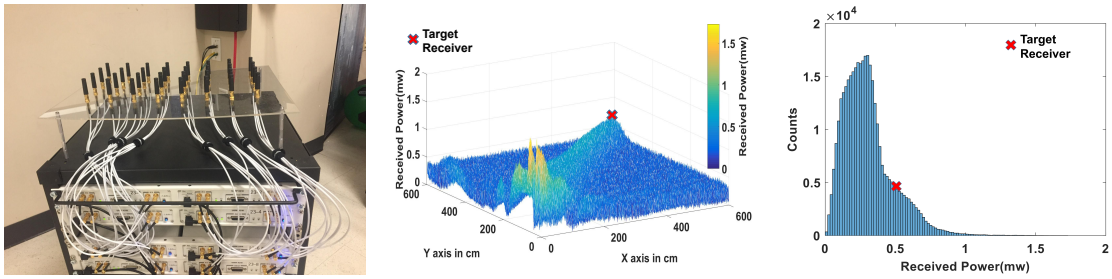

(a) (b) (c)

Fig. 14. Comparison experiments show the energy distribution of beamforming WPT systems. (a) Real world set up of our 16 by 16 beamforming USRP Rack. (b) Measured received power in the area between the beamforming rack and target receiver. (c) Statistics of measured power, there are still lots of locations have received power greater than the target receiver.

radio environment around the receiver stable within this period. Performing parallel measurements with multiple USRPs is not a viable approach either, due to differences in their hardware.

We thus use a specifically designed robot to address this challenge. The receiver's antenna is attached onto the robot. In this method, as soon as the phase combining at the receiver stabilizes, we stop the receiver from sending feedback messages. As a result, the locked phases at the transmitters lead to coherent phase combining at the original receiver's location. Next the robot will traverse the intended scanning area by a preset trace, which will cover the intended area as much as possible. Meanwhile the receiving USRP is recording the RSS during the whole process, and the RSS values are eventually mapped to their corresponding locations by comparing the timing information of the robot and the receiving USRP. During our experiment, we also make sure that the observed $RSS_{combined}$ value at the energy delivery destination (the original receiver location) does not have noticeable variation.

Results: In our topology (shown in Figure 9), we have measured a 6×6 m^2 (this size is limited by the maximum length of the coax cable) rectangular area around the receiver. Figure 13 (a) shows the measured received power distribution in a 3D view. We clearly witness a sharp energy peak around the target receiver location, while the energy at other locations are very low. Figure 13(b) shows the statistics of measured received power from the robot: the received power at target receiver is 0.63mw, which is the maximum received power of all measured spots. 62% of measured received power is less than 0.063mw and 99% of measured received power is less than 0.31mw.

As far as the MRC beamforming based WPT is concerned, Figure 14(b) shows the measured received power distribution. A strong energy beam projects toward the target receiver, and most of the received powers (89% of measured locations on the line of main beam) on this beam are higher than the received power at the target receiver. Figure 14(c) shows its statistics: received power at target receiver is 0.54mw, but there are 8% of measured spots have received power higher than the target receiver.

We note that on our facility, we cannot move these USRP antennas around, and as a result, the distances between the transmitters and the receiver in these two systems are different. Because of this, it is hard for us to directly compare the delivered power amount in both systems, nor can we compare their charging efficiency. However, we do see that these two systems lead to very different energy density distribution patterns. *Energy-Ball* has the energy peak only at the target receiver. Specifically, the peak/average received power ratio in this experiment is 8.72. As we noted in Section 2.2, these patterns potentially have different implications on safety of the system especially when the delivered energy amount goes up.

5.2 *Energy-Ball* Delivers Energy at Any Point across the Room

We have built a 20×20 m^2 area testbed. We now show *Energy-Ball* can align phases and delivery energy at any point within this area. For this purpose, we place the target receiver at 42 different locations, measure the delivered energy at each spot, and show the results in Figure 15. Among these 42 locations, location 1 is the center of the charging area while the other 41 locations are randomly chosen. Specifically, the received power at location 1 is $0.57mw$. When we move the receiver to a different location, our system re-align transmitters' phases. Experiment results show they all converge to over 90% of the optimal received power. Among these 42 measurements, the minimum, average and maximum received power are $0.51mw$, $0.63mw$ and $0.74mw$, respectively.

5.3 *Energy-Ball* Charges Mobile Receivers

Next, we show that our *Energy-Ball* testbed can successfully deliver energy to a mobile receiver as well. In this experiment, the trajectory of the mobile receiver is unknown to the transmitters.

Experimental Setup: We mount the receiver on our robot that moves on a straight line at constant speeds, 0.1, 0.2, 0.3, 0.4, 0.5 m/s. Here, as shown in Figure 16(a), while the robot is stationary, we first measure optimal

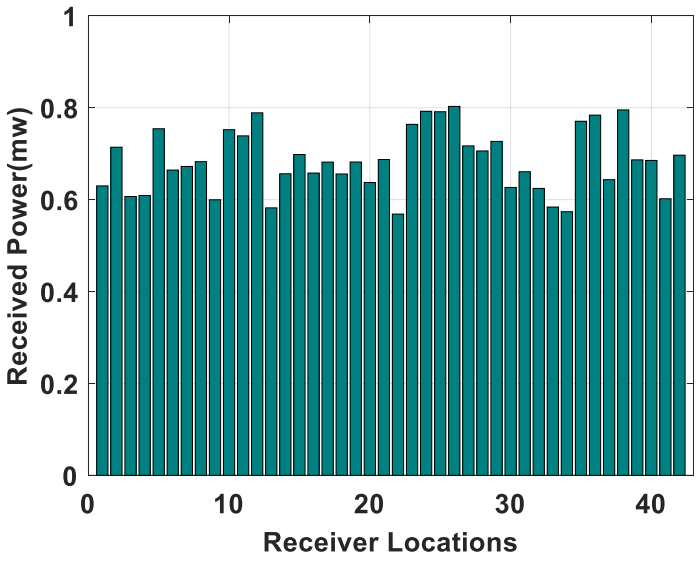

Fig. 15. In our 20×20 m^2 test area, we place the *Energy-Ball* receiver at 42 locations, in which location 1 is the center of the area and the other 41 locations are randomly chosen. We show the received power at each of these receiver locations here. Results show the received power at most of the locations is higher than the received power level at the center of the deployment area (location 1).

energies at 13 different positions along each moving track of 0.6m. Then the robot starts moving on a straight line as well as running *Energy-Ball*. We did this experiment for 13 times at each speed. The receiving USRP records received power data on the target receiver while the robot is moving. We use the average of 13 optimal measured energy as reference (100%), we compare the received power among (1) different moving speeds and (2) the performance between *Energy-Ball* is working and *Energy-Ball* is not turning on.

Results: Figure 16(b) shows around 80% of optimal received power is received for mobile receiver while *Energy-Ball* is working, only 14.7% of optimal received power is received while we turn off *Energy-Ball*. The adaptive Kalman filter design enables the mobile target receives significantly more energy, which is comparable with optimal energy (when the receiver is stationary). This result also suggests the received power under these 5 different tested speeds are similar.

5.4 Application Example- Charging Low-Power PIPs Sensors

Lastly, in this subsection, we provide evaluation results of charging PIPs (hardware details are given in Section 4) through a Powercast P2110-EVB harvester. With the delivered energy, we show that the PIPs sensor board is able to work without battery.

Enabling Battery-less IoT: In this experiment, we place PIPs in 13 randomly chosen locations in the charging area. At all 13 locations, *Energy-Ball* delivers over $0.6mw$ power that enables PIPs sensing and transmitting data continuously. The measured minimum, average and maximum received power across the room are $0.61mw$, $0.67mw$ and $0.79mw$ respectively. Figure 17(a) shows a portion of the reported sensor data from the sensor charged by our testbed. We observe no dropped packet during the entire experiment.

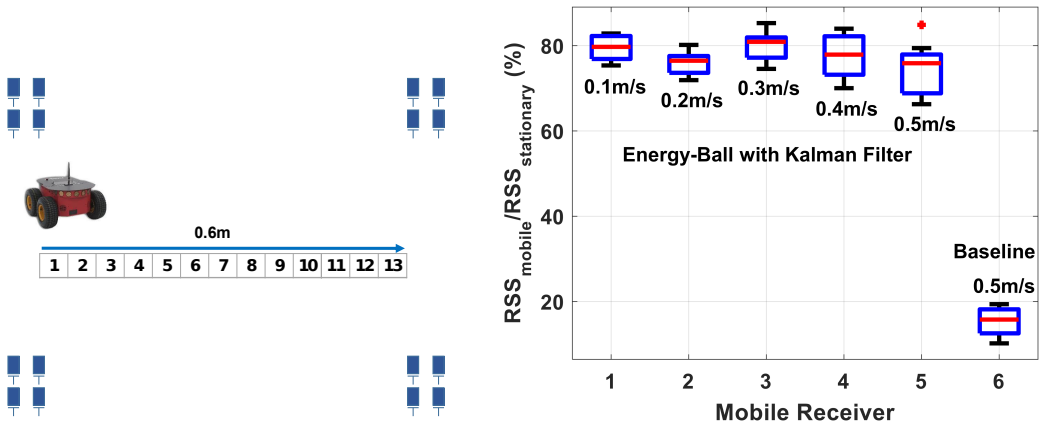

(a) (b)

Fig. 16. (a) We place the receiver on the robot, which moves at a constant speed along a 0.6 meter long trajectory. We measure received power at 13 different positions on the trajectory (transmitters are placed at 4 corners). (b) The received power percentage values at the mobile receiver with different moving speeds. The rightmost box represents the received power percentage value when *Energy-Ball* is turned off (transmitter phases are still aligned to the original receiver location).

Powering Specific PIPs through Precise Energy Delivery: Next we place the harvester and PIPs in location 7-14 (red square in Figure 17(b), O in Figure 17(c)). After a short charging period, the PIPs board is powered and begin to collect/report data continuously. Again, we observe no packet drop during the entire experimentation period.

With transmitters' phases locked, we move the harvester and PIPs to other locations (we move PIPs's location instead of having a different sensor at that location because we don't have enough number of power harvesters):

- *A short distance (wavelength 30cm) away from the energy focus.* We move the PIPs one λ (around 30 cm) away from the focus point O, i.e., A, B, C, D in Figure 17(c) (still within the red square in Figure 17(b). At these locations, the harvester can be charged slowly but PIPs fails to work continuously. For example at location A, PIPs could work for 90 seconds then it is down for a 20 minutes to charge, because the charging speed of P2110-EVB's on board energy storing capacitor is less than the rate of energy being consumed.
- *Farther away from the energy focus.* Next, we move the harvester and PIPs further away, to locations 7-13, 7-12, 8-14, 9-14, 7-15, 7-16, 6-14, 5-14, 15-15, 13-16, 15-7, and 7-6, one by one. As expected, PIPs did not get charged to a level where it could sense/communicate. These locations are marked by blue squares in Figure 17(b), and summarized as 'others' in Figure 17(c).

End-to-end Efficiency: Since our transmitters work in far-field settings, the end-to-end energy transferring efficiency ($p_{rx}/\Sigma p_{tx}$) is rather low, ranging from 1/1000 to 1/3000 across our 20 by 20 meter testbed. However, it is the physical limitation of any far-field WPT system. The end-to-end efficiency could be increased by using directional transmitters. We argue that such an energy delivery system is still valuable, mainly because the value of transmitted power and the value of received power is often asymmetric, especially if the receiving node is in a hard-to-access region. As IoT devices are made increasingly low-power, this concern becomes less severe.

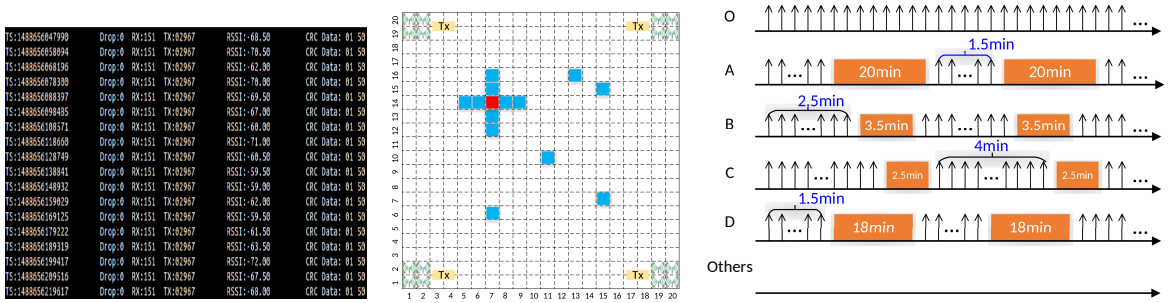

(a) (b) (c)

Fig. 17. In this experiment, we investigate whether sensors at locations other than the target can be powered. (a) Data reported by PIPs, including timestamp, dropped packet ID, server ID, sensor ID, RSSI and sensed data. (b) shows the experiment set up where the target sensor (O) is in the center of the red block, and A, B, C, and D are within the red blocks, 30cm away from O, and a few others are located in the blue squares. (c) shows how sensors at different locations operate when the energy is focused at O. O can work perfectly, A-D can work partially even though they are only 30cm away, and those sensors that are placed in the blue blocks do not have sufficient power to sense or communicate.

6 CONCLUSION

In this paper, we present a new WPT approach that transfers wireless energy to intended receivers by arranging a group of distributed transmitters around the receiver and coherently combining their phases at the receiver. This approach is a departure from existing beamforming based WPT approaches which have high energy on the energy beam path. The key innovation of our approach is that it can maximize the received power solely at the receiver, and have low received power at other locations across the space. Through detailed evaluation using 21 USRP nodes across a $20 \times 20m^2$ area, we show that the proposed approach can maximize the power level at the target receiver, can deliver a consistent amount of power to any point in the area, can charge a mobile receiver, and can continuously power a low-power IoT node at any point across the area.

ACKNOWLEDGMENTS

We are grateful to the IMWUT/Ubicomp reviewers for their constructive critiques, and Ivan Seskar, for his invaluable comments, all of which have helped us greatly improve this paper. This work was supported in part by the U.S. National Science Foundation(NSF) under grant CNS-1404118, CNS-1443434 and CNS-1423020.

REFERENCES

[1] 2010. FCC part 15. https://www.gpo.gov/fdsys/pkg/CFR-2010-title47-vol1/pdf/CFR-2010-title47-vol1-part15.pdf. (2010).
[2] 2014. The next generation of robotic assembly lines are emerging. https://gigaom.com/2014/02/11/the-next-generation-of-robotic-assembly-lines-are-emerging/. (2014).
[3] 2015. Compare your daughterboard's data from. http://files.ettus.com/performance_data/. (2015).
[4] 2015. Robots, drones and heart-detectors: How disaster technology is saving lives. http://www.cnn.com/2015/08/24/us/robot-disaster-technology/. (2015).
[5] 2016. Agilent E4405B Spectrum Analyzer. (2016). http://literature.cdn.keysight.com/litweb/pdf/E4401-90473.pdf.
[6] 2016. Ossia Just Released a Wireless Charger Kit That Works Like Wifi. https://www.inverse.com/article/25268-ossia-cota-wireless-charging-wifi?utm_source=twitter&utm_medium=inverse&utm_campaign=organic. (2016).
[7] 2017. Agricultural Drones Relatively cheap drones with advanced sensors and imaging capabilities are giving farmers new ways to increase yields and reduce crop damage. https://www.technologyreview.com/s/526491/agricultural-drones/. (2017).
[8] 2017. Datasheet of Powercast P2110 harvester chip. https://www.powercastco.com/wp-content/uploads/2016/11/p2110-datasheet-rev-b.pdf. (2017).

[9] 2017. Definition on near and far field. https://en.wikipedia.org/wiki/Near_and_far_field. (2017).
[10] 2017. FCC approves first wireless 'power-at-a-distance' charging system. https://www.engadget.com/2017/12/26/fcc-approves-first-wireless-power-at-a-distance-charging-syste/,. (2017).
[11] 2017. Highly Resonant Wireless Power Transfer: Safe, Efficient, and over Distance. http://witricity.com/wp-content/uploads/2016/12/White_Paper_20161218.pdf,. (2017).
[12] 2017. OET Bulletin No. 65 (August 1997). https://www.fcc.gov/general/oet-bulletins-line. (2017).
[13] 2017. Pi wireless charging. https://www.picharging.com/,. (2017).
[14] 2017. Pioneer P3-DX robot. http://www.mobilerobots.com/ResearchRobots/PioneerP3DX.aspx. (2017).
[15] Quentin Bonnard, Guillaume Zufferey, Andrea Mazzei, Sebastien Cuendet, Nan Li, and Pierre Dillenbourg. 2013. Chilitags: Robust Fiducial Markers for Augmented Reality. *CHILI, EPFL, Switzerland* (2013).
[16] William C Brown. 1965. *Experimental airborne microwave supported platform.* Technical Report. DTIC Document.
[17] Matthew J Chabalko, Mohsen Shahmohammadi, and Alanson P Sample. 2017. Quasistatic cavity resonance for ubiquitous wireless power transfer. *PloS ONE* 12, 2 (2017), e0169045.
[18] Peter WC Chan, Ernest S Lo, Ray R Wang, Edward KS Au, Vincent KN Lau, Roger S Cheng, Wai Ho Mow, Ross D Murch, and Khaled Ben Letaief. 2006. The evolution path of 4G networks: FDD or TDD? *IEEE Communications Magazine* 44, 12 (2006), 42–50.
[19] Haipeng Dai, Yunhuai Liu, Guihai Chen, Xiaobing Wu, and Tian He. 2014. Safe charging for wireless power transfer. In *INFOCOM, 2014 Proceedings IEEE*. IEEE, 1105–1113.
[20] Arthur P Dempster, Nan M Laird, and Donald B Rubin. 1977. Maximum likelihood from incomplete data via the EM algorithm. *Journal of the royal statistical society. Series B (methodological)* (1977), 1–38.
[21] Svenja Engels, Nils-Lasse Schneider, Nele Lefeldt, Christine Maira Hein, Manuela Zapka, Andreas Michalik, Dana Elbers, Achim Kittel, PJ Hore, and Henrik Mouritsen. 2014. Anthropogenic electromagnetic noise disrupts magnetic compass orientation in a migratory bird. *Nature* 509, 7500 (2014), 353–356.
[22] WTYZRH Xiaoran Fan, Zhijie Zhang, and Z Han. 2018. Secret-focus: A practical physical layer secret communication system by perturbing focused phases in distributed beamforming. INFOCOM.
[23] Bernhard Firner, Shweta Medhekar, Yanyong Zhang, Richard Howard, Wade Trappe, Peter Wolniansky, and Eitan Fenson. 2008. Pip tags: Hardware design and power optimization. In *Proceedings of HotEmNets*.
[24] Bernhard Firner, Robert S Moore, Richard Howard, Richard P Martin, and Yanyong Zhang. 2011. Poster: Smart buildings, sensor networks, and the internet of things. In *Proceedings of the 9th ACM Conference on Embedded Networked Sensor Systems*. ACM, 337–338.
[25] Om P Gandhi, L Lloyd Morgan, Alvaro Augusto de Salles, Yueh-Ying Han, Ronald B Herberman, and Devra Lee Davis. 2012. Exposure limits: the underestimation of absorbed cell phone radiation, especially in children. *Electromagnetic Biology and Medicine* 31, 1 (2012), 34–51.
[26] Maria Gorlatova, Robert Margolies, John Sarik, Gerald Stanje, Jianxun Zhu, Baradwaj Vigraham, Marcin Szczodrak, Luca Carloni, Peter Kinget, Ioannis Kymissis, et al. 2013. Prototyping energy harvesting active networked tags (EnHANTs). In *Proceedings of IEEE INFOCOM*.
[27] MA Graule, P Chirarattananon, SB Fuller, NT Jafferis, KY Ma, M Spenko, R Kornbluh, and RJ Wood. 2016. Perching and takeoff of a robotic insect on overhangs using switchable electrostatic adhesion. *Science* 352, 6288 (2016), 978–982.
[28] Brent Griffin and Carrick Detweiler. 2012. Resonant wireless power transfer to ground sensors from a UAV. In *Robotics and Automation (ICRA), 2012 IEEE International Conference on*. IEEE, 2660–2665.
[29] Jiann-Ching Guey and L Daniel Larsson. 2004. Modeling and evaluation of MIMO systems exploiting channel reciprocity in TDD mode. In *Vehicular Technology Conference, 2004. VTC2004-Fall. 2004 IEEE 60th*, Vol. 6. IEEE, 4265–4269.
[30] Maxime Guillaud, Dirk TM Slock, and Raymond Knopp. 2005. A practical method for wireless channel reciprocity exploitation through relative calibration.. In *ISSPA*. 403–406.
[31] Yantao Han, Jiqing Ni, and Gaoke Du. 2010. The potential approaches to achieve channel reciprocity in FDD system with frequency correction algorithms. In *Communications and Networking in China (CHINACOM), 2010 5th International ICST Conference on*. IEEE, 1–5.
[32] Magda Havas, Jeffrey Marrongelle, Bernard Pollner, Elizabeth Kelley, Camilla RG Rees, and Lisa Tully. 2010. Provocation study using heart rate variability shows microwave radiation from 2.4 GHz cordless phone affects autonomic nervous system. *European Journal of Oncology Library* 5 (2010), 273–300.
[33] Vikram Iyer, Elyas Bayati, Rajalakshmi Nandakumar, Arka Majumdar, and Shyamnath Gollakota. 2018. Charging a Smartphone Across a Room Using Lasers. *Proceedings of the ACM on Interactive, Mobile, Wearable and Ubiquitous Technologies* 1, 4 (2018), 143.
[34] Jouya Jadidian and Dina Katabi. 2014. Magnetic MIMO: How to charge your phone in your pocket. In *Proceedings of ACM MobiCom*.
[35] Florian Kaltenberger, Haiyong Jiang, Maxime Guillaud, and Raymond Knopp. 2010. Relative channel reciprocity calibration in MIMO/TDD systems. In *Future Network and Mobile Summit, 2010*. IEEE, 1–10.
[36] Sanghoek Kim, John S Ho, and Ada SY Poon. 2012. Wireless power transfer to miniature implants: Transmitter optimization. *IEEE Transactions on Antennas and Propagation* 60, 10 (2012), 4838–4845.
[37] Joseph L Kirschvink. 2014. Sensory biology: Radio waves zap the biomagnetic compass. *Nature* 509, 7500 (2014), 296–297.

[38] Hamid Krim and Mats Viberg. 1996. Two decades of array signal processing research: the parametric approach. *IEEE Signal Processing Magazine* 13, 4 (1996), 67–94.
[39] Vincent Liu, Aaron Parks, Vamsi Talla, Shyamnath Gollakota, David Wetherall, and Joshua R Smith. 2013. Ambient backscatter: wireless communication out of thin air. *ACM SIGCOMM Computer Communication Review* 43, 4 (2013), 39–50.
[40] Xiao Lu, Ping Wang, Dusit Niyato, Dong In Kim, and Zhu Han. 2016. Wireless charging technologies: Fundamentals, standards, and network applications. *IEEE Communications Surveys & Tutorials* 18, 2 (2016), 1413–1452.
[41] Adelina Madhja, Sotiris Nikoletseas, and Theofanis P Raptis. 2015. Distributed wireless power transfer in sensor networks with multiple mobile chargers. *Computer Networks* 80 (2015), 89–108.
[42] Utz Martin and Michael Grigat. 1996. A statistical simulation model for the directional mobile radio channel and its configuration. In *Spread Spectrum Techniques and Applications Proceedings, 1996., IEEE 4th International Symposium on*, Vol. 1. IEEE, 86–90.
[43] Gregory Melia. 2013. *Electromagnetic Absorption by the Human Body from 1-15 GHz.* Ph.D. Dissertation. University of York.
[44] Mohammad Reza Vedady Moghadam and Rui Zhang. 2017. Node placement and distributed magnetic beamforming optimization for wireless power transfer. *IEEE Transactions on Signal and Information Processing over Networks* (2017).
[45] Raghuraman Mudumbai, Joao Hespanha, Upamanyu Madhow, and Gwen Barriac. 2005. Scalable feedback control for distributed beamforming in sensor networks. In *Proceedings of IEEE ISIT*.
[46] Raghuraman Mudumbai, Ben Wild, Upamanyu Madhow, and Kannan Ramchandran. 2006. Distributed beamforming using 1 bit feedback: from concept to realization. In *Proceedings of Citeseer Allerton*.
[47] Ufuk Muncuk, Subhramoy Mohanti, Kubra Alemdar, M Yousof Naderi, and Kaushik R Chowdhury. 2016. Software-defined Wireless Charging of Internet of Things using Distributed Beamforming: Demo Abstract. In *Proceedings of the 14th ACM Conference on Embedded Network Sensor Systems CD-ROM*. ACM, 326–327.
[48] Henrietta Nittby, Bengt Widegren, Morten Krogh, Gustav Grafström, Henrik Berlin, Gustav Rehn, Jacob L Eberhardt, Lars Malmgren, Bertil RR Persson, and Leif G Salford. 2008. Exposure to radiation from global system for mobile communications at 1,800 MHz significantly changes gene expression in rat hippocampus and cortex. *The Environmentalist* 28, 4 (2008), 458–465.
[49] Maria P Ntzouni, Aikaterini Skouroliakou, Nikolaos Kostomitsopoulos, and Lukas H Margaritis. 2013. Transient and cumulative memory impairments induced by GSM 1.8 GHz cell phone signal in a mouse model. *Electromagnetic biology and medicine* 32, 1 (2013), 95–120.
[50] Arogyaswami J Paulraj, Dhananjay A Gore, Rohit U Nabar, and Helmut Bolcskei. 2004. An overview of MIMO communications-a key to gigabit wireless. *Proc. IEEE* 92, 2 (2004), 198–218.
[51] Morgan Quigley, Ken Conley, Brian Gerkey, Josh Faust, Tully Foote, Jeremy Leibs, Rob Wheeler, and Andrew Y Ng. 2009. ROS: an open-source Robot Operating System. In *ICRA workshop on open source software*, Vol. 3. Kobe, 5.
[52] François Quitin, Upamanyu Madhow, Muhammad Mahboob Ur Rahman, and Raghuraman Mudumbai. 2012. Demonstrating distributed transmit beamforming with software-defined radios. In *Proceedings of IEEE WoWMoM*.
[53] François Quitin, Muhammad Mahboob Ur Rahman, Raghuraman Mudumbai, and Upamanyu Madhow. 2012. Distributed beamforming with software-defined radios: frequency synchronization and digital feedback. In *Proceedings of IEEE GLOBECOM*.
[54] Ryan Rogalin, Ozgun Y Bursalioglu, Haralabos Papadopoulos, Giuseppe Caire, Andreas F Molisch, Antonios Michaloliakos, Vlad Balan, and Konstantinos Psounis. 2014. Scalable synchronization and reciprocity calibration for distributed multiuser MIMO. *IEEE Transactions on Wireless Communications* 13, 4 (2014), 1815–1831.
[55] Vamsi Talla, Bryce Kellogg, Benjamin Ransford, Saman Naderiparizi, Shyamnath Gollakota, and Joshua R Smith. 2015. Powering the next billion devices with Wi-Fi. In *Proceedings of the 11th ACM Conference on Emerging Networking Experiments and Technologies*. ACM, 4.
[56] Peter JM Van Laarhoven and Emile HL Aarts. 1987. Simulated annealing. In *Simulated annealing: Theory and applications*. Springer, 7–15.
[57] Rui Wang, Radu David, and D Richard Brown. 2015. Feedback rate optimization in receiver-coordinated distributed transmit beamforming for wireless power transfer. In *Information Sciences and Systems (CISS), 2015 49th Annual Conference on*. IEEE, 1–6.
[58] Tao Wang, Yao Liu, and Athanasios V Vasilakos. 2015. Survey on channel reciprocity based key establishment techniques for wireless systems. *Wireless Networks* 21, 6 (2015), 1835–1846.
[59] Fei Zhang, Steven A Hackworth, Xiaoyu Liu, Haiyan Chen, Robert J Sclabassi, and Mingui Sun. 2009. Wireless energy transfer platform for medical sensors and implantable devices. In *Proceedings of IEEE EMBC*.
[60] Yanyong Zhang, Bernhard Firner, Richard Howard, Richard Martin, Narayan Mandayam, Junichiro Fukuyama, and Chenren Xu. 2017. Transmit Only: An Ultra Low Overhead MAC Protocol for Dense Wireless Systems. In *Smart Computing (SMARTCOMP), 2017 IEEE International Conference on*. IEEE, 1–8.

Received November 2017; revised February 2018; accepted April 2018